ChemComm

COMMUNICATION

View Article Online
View Journal | View Issue

Cite this: *Chem. Commun.*, 2025, **61**, 15227

Received 23rd May 2025,
Accepted 26th August 2025

DOI: 10.1039/d5cc02423d

rsc.li/chemcomm

Dynamic membranization results in core–shell coacervates that selectively localize particles and small molecules

Tsvetomir Ivanov, [a] Shoupeng Cao, [ab] Maximilian Schaaf, [a] Lucas Caire da Silva *[ac] and Katharina Landfester *[a]

We present a dynamic multiphase coacervate system that enables selective molecular partitioning, mimicking cellular compartmentalization. This pH-responsive platform separates enzymatic products based on polarity and exhibits enhanced colloidal stability for prolonged use. These advances position multiphase coacervates as robust tools for catalysis, synthetic biology, and bio-inspired chemical systems.

Liquid–liquid phase separation (LLPS) of biological molecules facilitates the formation of membraneless organelles within living cells, contributing to the organization of cellular contents, molecular exchange, and regulation of biochemical processes.[1–4] A key feature of these biological assemblies is their reversible formation and dissolution in response to biochemical processes, such as post-translational modifications or DNA transcription. This dynamic behaviour enables precise spatial and temporal compartmentalization, which is critical for cellular coordination, adaptation, and signal transduction.[5–9]

Inspired by nature, *in vitro* coacervation has emerged as a versatile approach for constructing synthetic analogues of membraneless organelles. This method has applications in fields such as drug delivery, biosensing, and artificial cells. The complexity of an *in vitro* coacervation can be categorized as either simple or complex, depending on whether the interactions between components are segregative or associative. Complex coacervation, driven by attractive interactions between macromolecules like polysaccharides, polypeptides, or synthetic polymers, typically produces droplets with a homogeneous single phase.[10–14] Recent studies have demonstrated the potential of multiphase coacervates, which form *via* the combination of three or more components, creating multicompartmentalized, droplet-in-droplet configuration.[15–18] Properties such as selective molecular partitioning, adaptability and cell-like structural organization make multiphase droplets promising for applications as artificial cells and platforms for cell-like microreactors.[19–23] Dynamic assembly of multiphase systems has also been explored. Martin *et al.* developed enzyme-driven systems that self-assemble and dissolve based on pH shifts, enabling precise control over droplet formation.[18] For instance, the Spruijt and Keating groups demonstrated the formation of hierarchically organized multiphase droplets.[17,24] Despite progress in the development of static structures, engineering adaptable and dynamic multiphase systems with stimuli-responsive architectures remains a significant challenge. Moreover, current systems often suffer from poor colloidal stability due to the absence of a protective membrane, limiting their effectiveness and longevity as robust bio-inspired platforms.

In this work, we describe a stable, dynamic multiphase coacervate system. The core of the droplet comprises adenosine triphosphate (ATP) and α-poly-L-lysine (PLL), oppositely charged molecules forming a pH-stable core. Surrounding the core is a membrane layer of diethylaminoethyl-dextran (DEX) and carboxy-amylose (AMC), a pair chosen for its pH responsiveness. The system enables selective molecular partitioning based on charge and polarity within its layers. To form pH-responsive multiphase coacervates, two pairs of oppositely charged components were selected: ATP and PLL for the core, and DEX and AMC for the shell (Fig. 1a). ATP/PLL droplets form stable coacervates across a pH range of 5 to 10 (Fig. S1), while DEX/AMC droplets form coacervates between pH 4 and 9 (Fig. S2). The phase behavior of the core and shell pairs at room temperature was tested by mixing stock solutions of 5 mg mL^{-1} for each component at a 1 : 1 volume ratio in 5 mM HEPES with pH 6. Under these conditions, AMC and PLL formed small droplets with diameters of approximately 1 μm (Fig. S3), while ATP and DEX did not form droplets. As expected, ATP/AMC and DEX/PLL did not form droplets because of electrostatic repulsion (Fig. S3). A stable three-

[a] *Department Physical Chemistry of Polymers, Max Planck Institute for Polymer Research, Ackermannweg 10, 55128 Mainz, Germany. E-mail: landfester@mpip-mainz.mpg.de*
[b] *College of Polymer Science and Engineering, National Key Laboratory of Advanced Polymer Materials, Sichuan University, Chengdu 610065, P. R. China*
[c] *Department of Chemistry, McGill University, Montreal, H3A 0B8, Canada. E-mail: lucas.cairedasilva@mcgill.ca*

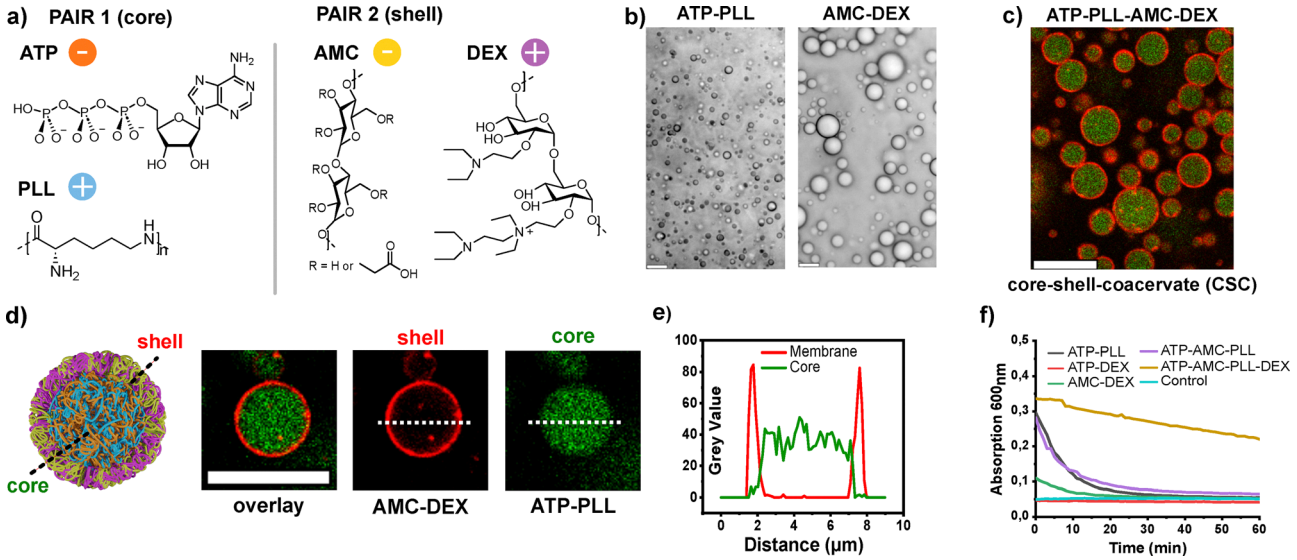

Fig. 1 Formation and characterization of single-phase and core–shell-coacervate droplets. (a) Chemical structures of coacervate components: anionic ATP and AMC, cationic PLL and DEX; (b) brightfield microscopy of ATP–PLL and AMC–DEX (1 : 1, 5 mg mL^{-1}, 5 mM HEPES, pH ~ 7). (c) Confocal microscopy of core–shell coacervates (1 : 1 : 1 : 1), with FITC-labeled core and Rhodamine B-labeled shell. (d) Schematic and CLSM images of ATP/PLL/AMC/DEX core–shell structure. (e) Fluorescence profile of a single droplet showing core–shell organization. (f) Turbidity-based stability analysis of individual coacervate compositions (5 mg mL^{-1} each, 5 mM HEPES). Scale bars = 10 μm.

component system of ATP/PLL/AMC formed homogenous droplets with diameters of *ca.* 15 μm (Fig. S3–S9). However, a three-component system comprised of ATP/PLL/DEX resulted in ATP–PLL droplets with freely distributed DEX within the inner volume of the coacervates and the outer medium, as DEX could not effectively interact with other components (Fig. S10). A four-component coacervate system was successfully assembled by sequentially adding positively charged polyelectrolytes (DEX and PLL) followed by negatively charged components (ATP and AMC) (Fig. 1c). This resulted in a core–shell structure, where the shell thickness could be adjusted by increasing the fraction of DEX (Fig. S11). A 1 : 1 : 1 : 1 volume ratio (global composition) produced a thin shell (around 0.4 μm) resembling a membrane surrounding the core (Fig. 1c). This volume ratio corresponds to a global positive-to-negative charge ratio of approximately 1.1, indicating a slight excess of positive charges. The fluidity of the core–shell droplets was investigated using fluorescence recovery after photobleaching (FRAP). Both the shell and the core phases exhibited near complete fluorescence recovery within approximately 60 s after photobleaching, confirming their dynamic and liquid-like nature (Fig. S22). We refer to this system as core–shell coacervates (CSCs). Due to the enhanced colloidal stability, all CSCs were formulated using a 1 : 1 : 1 : 1 volume ratio. The spatial distribution of each component was investigated using fluorescent probes. FITC-labeled PLL revealed that PLL localizes within the droplet core, while Rhodamine-labeled DEX indicated that DEX is predominantly localized in the shell (Fig. 1d). Additionally, BDP-labeled AMC showed a homogeneous distribution throughout the entire droplet volume (Fig. S12). The observed distribution of components arises from the partial immiscibility of the components and differences in interfacial tensions.[17]

Complex coacervates are prone to coalescence, often merging within minutes to form a bulk liquid phase. Single-phase ATP/PLL droplets merged within seconds (Fig. S13). However, the core–shell ATP/PLL/AMC/DEX droplets (CSC) showed improved stability, resisting coalescence up to 24 h under sealed conditions (Fig. S14 and S15). Enhanced stability against dilution was also observed. CSCs persisted at polymer concentrations as low as 1 mg mL^{-1}, while single-phase droplets showed signs of wetting to the glass surface and dissolving below 2 mg mL^{-1} (Fig. S15). The presence of the shell reduced the tendency of droplets to merge and wet surfaces. The colloidal stability was assessed using turbidity measurements over time (Fig. 1). Colloidal stability was assessed using turbidimetry, where decreases in absorbance indicate loss of suspended droplets *via* interfacial wetting or sedimentation (Fig. 1f). All systems except the CSC formulation exhibited a rapid drop in absorbance within minutes, consistent with wetting and drainage. In contrast, the CSC formulation showed only a gradual decrease over more than 60 min, indicating superior resistance to fusion and wetting. This stabilization is attributed to the DEX-rich outer membrane, which enhances CSC colloidal stability through electrostatic repulsion and hydration effects. To evaluate the effect of composition on surface charge, zeta potential measurements were performed on the droplets (Fig. S16). ATP/PLL droplets had a potential of +18 mV, while AMC/DEX droplets had a potential of −5 mV. The three-component ATP/PLL/AMC system had a high negative potential (−17 mV). CSCs showed a zeta potential of around +10 mV, consistent with the slightly positive global charge ratio (1.1) dominated by DEX. Coacervate droplets can form and disassemble in response to external stimuli such as temperature, light, pH value, or concentration.[10,25] In our system, the pH-responsiveness of the DEX component (pK_a 9.2) in the core–shell droplet enables dynamic disassembly of the shell while maintaining overall droplet integrity. Under basic conditions, deprotonation of these

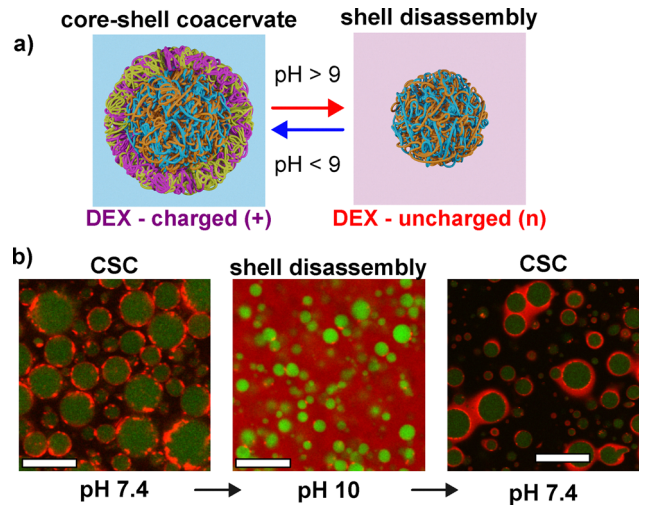

Fig. 2 Reversible formation and disassembly of CSCs. (a) Schematic representation of assembly and disassembly; (b) the droplet core is visualized through PLL-FITC, while the shell is observed *via* DEX-Rhod.; scale bar = 10 μm.

groups reduces the charge density required for interaction with AMC.

Lowering the pH below 9 restores the positive charge of DEX, enabling electrostatic interaction with AMC. The CSC dynamics were visualized with Rhodamine-labeled DEX (shell) and FITC-labeled PLL (core). At pH 7.4, DEX localized at the shell as expected. When the pH was increased to 10, DEX became uncharged and dispersed into the surrounding medium. Upon returning the pH to 7.4 and gently mixing, DEX reassembled into the membrane layer, demonstrating reversible and pH-responsive dynamic behavior (Fig. 2a and b). The selectivity of the shell and core for cargoes was evaluated by studying the partitioning *via* confocal laser microscopy. All coacervate components were maintained at a constant concentration of 5 mg mL^{-1}. Nile-red (hydrophobic) localized exclusively to the core, whereas FITC-BSA (anionic, high-MW) was confined to the shell (Fig. 3a and Fig. S17). The positive ζ-potential of the CSCs and the enrichment of cationic DEAE-dextran relative to anionic AMC is believed to drive electrostatic recruitment of BSA to the shell, yielding clear core–shell selectivity. The effective mesh size of the dense ATP/PLL coacervate also favors interfacial/shell localization over core entry. Due to the pH-responsive nature of the shell, the localization of the macromolecular cargo can be dynamically controlled by reversibly recruiting or releasing FITC-BSA (Fig. 3b and c). Selectivity for small molecules (<500 g mol^{-1}) strongly depends on their charge and ability to engage in weak binding interactions, such as π–π and cation–π interactions. For instance, fluorescein, a hydrophilic dianion, exhibits high affinity for the CSC shell, primarily due to the highly hydrated and positively charged environment provided by DEAE-dextran (Fig. 4b). In contrast, less charged molecules capable of weak hydrophobic interactions with ATP and PLL tend to localize within the core (Fig. S23). The ability to spatially co-localize reaction products within distinct layers of the core–shell system was also investigated. To demonstrate this functionality, two enzymatic reactions were performed. In the first reaction, the

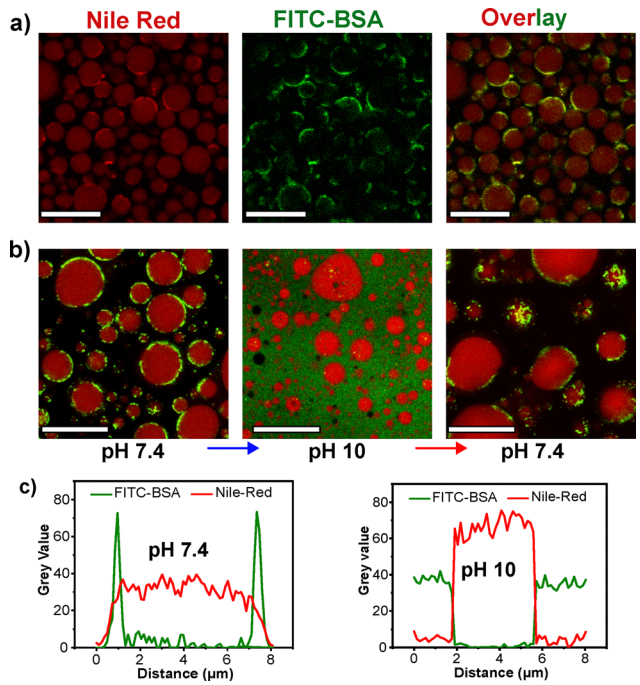

Fig. 3 Distribution of hydrophobic and macromolecular cargo in CSCs. (a) Distribution at constant pH; (b) pH-induced release of macromolecular cargo; (c) fluorescence profile of CSCs. All coacervate components at 5 mg mL^{-1}. Scale bar = 10 μm.

enzyme horseradish peroxidase (HRP) was encapsulated within CSC system (Fig. 4a). Hydrogen peroxide and Amplex Red were added to the droplet exterior, resulting in the synthesis of the fluorescent hydrophobic product resorufin. This product remained localized within the coacervate droplet during the enzymatic reaction (Fig. 4a). In the second reaction, the enzyme β-galactosidase was encapsulated within the coacervate system. When fluorescein-di-β-D-galactopyranoside (FDG) was introduced into the surrounding medium, β-galactosidase hydrolyzed the glycosidic bond between fluorescein and galactose, forming the negatively charged fluorescent product fluorescein, localized primarily within the positively charged shell (Fig. 4b and Fig. S21). An additional advantage of the CSC core–shell structure is its ability to reconfigure the localization of nano-objects in response to coacervate composition. We demonstrate this by introducing small unilamellar vesicles (SUVs) composed of cholesterol, 1,2-dioleoyl-*sn-glycero*-3-phosphoethanolamine (DOPE), and L-α-phosphatidylcholine (EggPC) in a 1 : 1 : 1 molar ratio. These SUVs had a negative charge (ζ = −15 mV) and a hydrodynamic diameter of about 100 nm (Fig. S18 and S19). In positively charged ATP/PLL droplets (+18 mV), SUVs were accumulated at the interface (Fig. 4c). SUVs were excluded from the dense ATP/PLL core due to its high charge density and small effective mesh size. When AMC is added, the droplet ζ-potential becomes negative (Fig. S16), driving SUVs toward the interface *via* electrostatic repulsion. Subsequent addition of DEAE-dextran forms a cationic shell that binds the interfacial SUVs and kinetically traps them as a peripheral ring. Transient heterogeneity during shell formation likely accounts for the observed SUV aggregates (Fig. 4c). In summary,

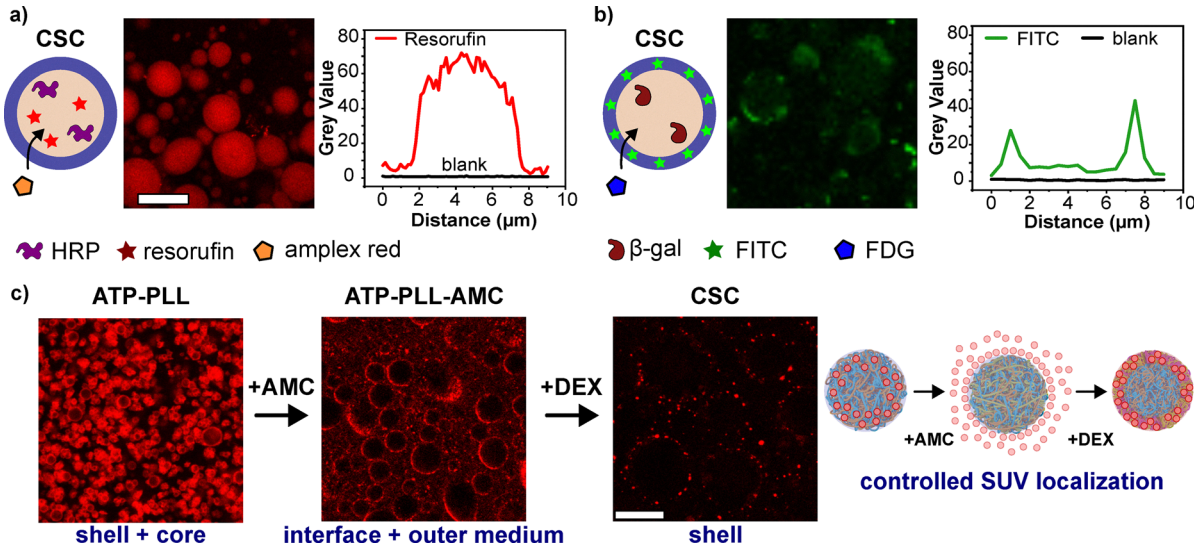

Fig. 4 Partitioning of chemical reaction products and large cargoes in CSCs. (a) Enzymatic reaction utilizing HRP for the synthesis of resorufin; (b) enzymatic reaction utilizing β-galactosidase for the synthesis of fluorescein; (c) partitioning of negatively-charged small unilamellar vesicles (SUV) in different coacervates systems, the ratio between the components after addition is maintained at 1 : 1 : 1 after AMC and 1 : 1 : 1 : 1 after DEX to a final concentration of 5 mg mL^{-1}. Scale bar = 10 μm.

this study has demonstrated the design and characterization of a dynamic core–shell complex coacervate system capable of selective molecular partitioning and controlled cargo release.

The system exploits the complementary properties of ATP/PLL for a stable core and DEX/AMC for a pH-responsive shell, allowing for reversible assembly and disassembly. Through spatial organization, the coacervates effectively separate hydrophobic and hydrophilic molecules and localize enzymatic reaction products in distinct compartments. In addition, the dynamic pH-responsiveness of the system allows precise control of molecule separation and release. These findings establish core–shell coacervates as a versatile platform for applications in synthetic biology, catalysis, and bio-inspired chemical systems.

This work was supported by the Max Planck Society and the Alexander von Humboldt Foundation. Open Access funding provided by the Max Planck Society.

Conflicts of interest

There are no conflicts of interest to declare.

Data availability

The data supporting this article have been included as part of the SI. See DOI: https://doi.org/10.1039/d5cc02423d

Notes and references

1 S. Alberti, A. Gladfelter and T. Mittag, *Cell*, 2019, **176**, 419–434.
2 D. T. Murray, M. Kato, Y. Lin, K. R. Thurber, I. Hung, S. L. McKnight and R. Tycko, *Cell*, 2017, **171**, 615–627.
3 S. Choi, M. C. O. Meyer, P. C. Bevilacqua and C. D. Keating, *Nat. Chem.*, 2022, **14**, 1110–1117.
4 C. Forenzo and J. Larsen, *Mol. Pharm.*, 2023, **20**, 4387–4403.
5 J. M. Iglesias-Artola, B. Drobot, M. Kar, A. W. Fritsch, H. Mutschler, T. Y. Dora Tang and M. Kreysing, *Nat. Chem.*, 2022, **14**, 407–416.
6 T. Lu, S. Javed, C. Bonfio and E. Spruijt, *Small Methods*, 2023, **7**, 2300294.
7 M. H. M. E. van Stevendaal, J. C. M. van Hest and A. F. Mason, *ChemSystemsChem*, 2021, **3**, e2100009.
8 V. Mukwaya, S. Mann and H. Dou, *Commun. Chem.*, 2021, **4**, 161.
9 C. Guindani, L. C. da Silva, S. Cao, T. Ivanov and K. Landfester, *Angew. Chem., Int. Ed.*, 2022, **61**, e202110855.
10 A. B. Cook, S. Novosedlik and J. C. M. van Hest, *Acc. Mater. Res.*, 2023, **4**, 287–298.
11 T. Ivanov, S. Cao, N. Bohra, M. de Souza Melchiors, L. Caire da Silva and K. Landfester, *ACS Appl. Mater. Interfaces*, 2023, **15**, 50755–50764.
12 S. Cao, T. Ivanov, J. Heuer, C. T. J. Ferguson, K. Landfester and L. Caire da Silva, *Nat. Commun.*, 2024, **15**, 39.
13 X. Liu, A. H. Mokarizadeh, A. Narayanan, P. Mane, A. Pandit, Y. M. Tseng, M. Tsige and A. Joy, *J. Am. Chem. Soc.*, 2023, **145**, 23109–23120.
14 G. B. Perin, S. Moreno, Y. Zhou, M. Günther, S. Boye, B. Voit, M. I. Felisberti and D. Appelhans, *Biomacromolecules*, 2023, **24**, 5807–5822.
15 Y. Chen, M. Yuan, Y. Zhang, S. Liu, X. Yang, K. Wang and J. Liu, *Chem. Sci.*, 2020, **11**, 8617–8625.
16 Y. Sun, S. Y. Lau, Z. W. Lim, S. C. Chang, F. Ghadessy, A. Partridge and A. Miserez, *Nat. Chem.*, 2022, **14**, 274–283.
17 T. Lu and E. Spruijt, *J. Am. Chem. Soc.*, 2020, **142**, 2905–2914.
18 H. Karoui, M. J. Seck and N. Martin, *Chem. Sci.*, 2021, **12**, 2794–2802.
19 I. B. A. Smokers, B. S. Visser, A. D. Slootbeek, W. T. S. Huck and E. Spruijt, *Acc. Chem. Res.*, 2024, **57**, 1885–1895.
20 W. Mu, L. Jia, M. Zhou, J. Wu, Y. Lin, S. Mann and Y. Qiao, *Nat. Chem.*, 2024, **16**, 158–167.
21 K. K. Nakashima, M. H. I. van Haren, A. A. M. André, I. Robu and E. Spruijt, *Nat. Commun.*, 2021, **12**, 3819.
22 J. Wang, M. Abbas, Y. Huang, J. Wang and Y. Li, *Commun. Chem.*, 2023, **6**, 243.
23 A. F. Mason, B. C. Buddingh, D. S. Williams and J. C. M. Van Hest, *J. Am. Chem. Soc.*, 2017, **139**, 17309–17312.
24 G. A. Mountain and C. D. Keating, *Biomacromolecules*, 2020, **21**, 630–640.
25 T. Ivanov, T. P. Doan-Nguyen, M. A. Belahouane, Z. Dai, S. Cao, K. Landfester and L. Caire da Silva, *Macromol. Rapid Commun.*, 2024, **45**, 2400626.

